Electronic Supplementary Material (ESI) for Materials Horizons.

Supplementary Information: Visualizing Defect Energetics

Shashwat Anand*, James P. Male, Chris Wolverton, and G. Jeffrey Snyder*

Department of Materials Science and Engineering, Northwestern University, Evanston

E-mail: sanand@lbl.gov

Chemical potential diagram construction from the convex-hull

The chemical potentials pertaining to various phase equilibria are needed for calculating point defect formation energies.[1–3] The range of such chemical potentials available for calculations can be directly visualized from a convex-hull construction (Figure S1). In the A-B model system, the energies at the y-intercepts of a "common-tangent" line on the A and B energy axes are $\Delta\mu_A$ and $\Delta\mu_B$, respectively. As an example, for AB in equilibrium with A (Figure S1a), the y-intercepts of the line between the two compounds gives $\Delta\mu_A = 0$ and $\Delta\mu_B < 0$, as expected in equilibrium with elemental A. Similarly, AB in equilibrium with B (Figure S1c) gives $\Delta\mu_B = 0$ and $\Delta\mu_A < 0$. A compound AB that is not in established equilibrium with either A or B (Figure S1b) will have both $\Delta\mu_A < 0, \Delta\mu_B < 0$.

Visualizing chemical potentials in the frequently used chemical potential space requires only the information from the convex-hull y-intercepts. In a typical binary chemical potential diagram, the x- and y-axes represent $\Delta\mu$ for each element (see right column of Figure S1). For the $A - B$ system with stable phases AB, A, and B, the two possible phase equilibria for AB are with elemental A ($\Delta\mu_A = 0$) or B ($\Delta\mu_B = 0$). Applying the common-tangent approach to the convex-hull, as described above, allows one to plot $\Delta\mu_A$ and $\Delta\mu_B$ for any

composition constrained by available phase equilibria. In chemical potential space, a line drawn through the results encompasses all accessible chemical potentials for the AB phase. A similar plot can be made for metastable AB_3. However, the magnitudes of $\Delta\mu_B$ and $\Delta\mu_A$ will be lower than those for compound AB across the entire composition range, indicating less favorable energetics for formation (Figure S1(a-c)). Only phases with the lowest-lying lines in chemical potential space are stable. Additionally, the slope of a line drawn in chemical potential space represents stoichiometry. In the example provided, the slope for phases AB and AB_3 are -1 and -1/4, respectively.

As additional phases "break" the convex-hull and become stable, they can reduce the range of accessible chemical potentials for other phases in the system. Following the example of Figure S1, when a phase AB_3 becomes stable (Figure S1d), the B-rich equilibrium for phase AB is no longer between AB and B - but rather between AB and AB_3. Correspondingly, the line representing AB_3 in chemical potential space (right column of Figure S1d) drops below that of AB, signifying that the AB phase is no longer stable at certain compositions. As a result, the lowest magnitude of $\Delta\mu_B$ in AB must be some finite value greater than 0.

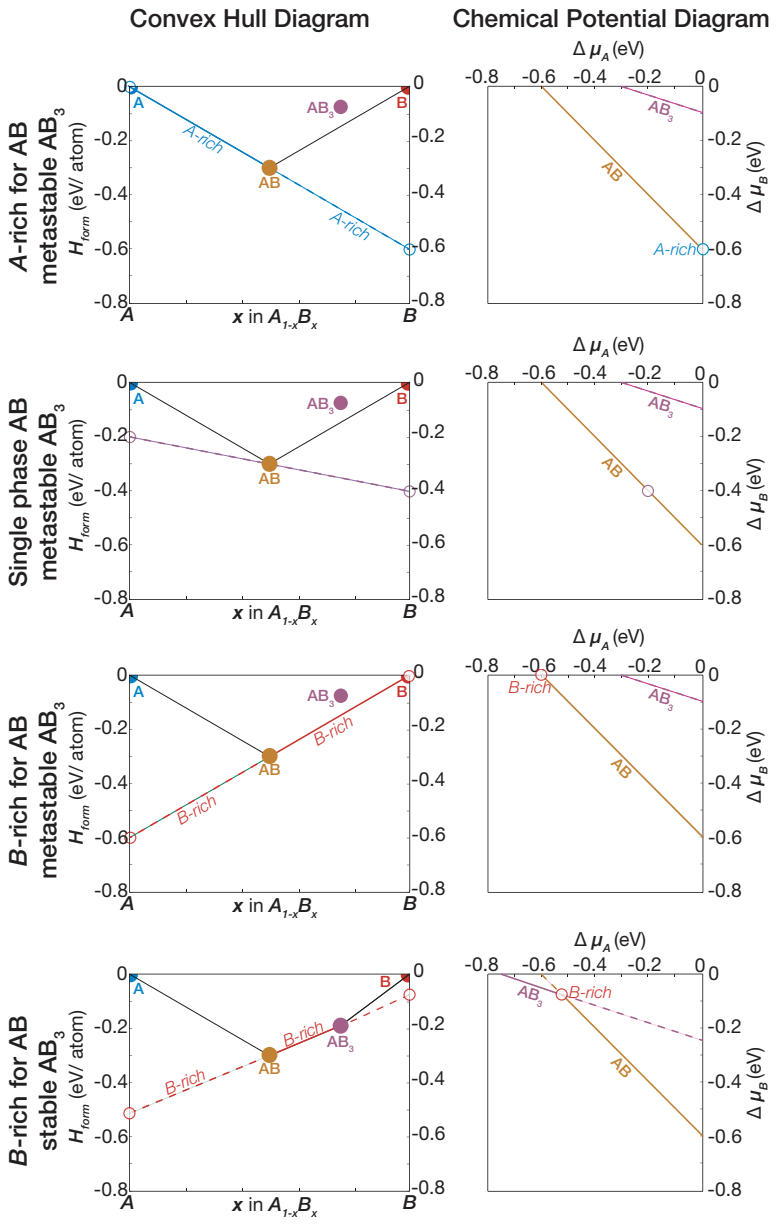

Figure S1: (a-c) A convex-hull construction for the hypothetical $A-B$ binary system (left column) with stable phases A, B, and AB and metastable phase AB_3. (a) When phase AB in in equilibrium with A ($\Delta\mu_A = 0$), the change in elemental chemical potentials, $\Delta\mu_A$ and $\Delta\mu_B$, are directly read from the y intercepts of the line connecting AB and B and plotted in chemical potential space (right column). (b) Shifting equilibrium from AB and A diverts $\Delta\mu_A$ and $\Delta\mu_B$ from their extrema until reaching equilibrium between AB and B (c), where $\Delta\mu_B = 0$. The line connecting every chemical potential between the two equilibria captures the entire range of accessible chemical potentials for AB. (d) When phase AB_3 become stable, the line representing its chemical potentials falls below that of phase AB in chemical potential space. Phase equilibrium between AB and B is no longer possible, and is replaced by equilibrium between AB and AB_3, reducing the range of $\Delta\mu_B$ accessible.

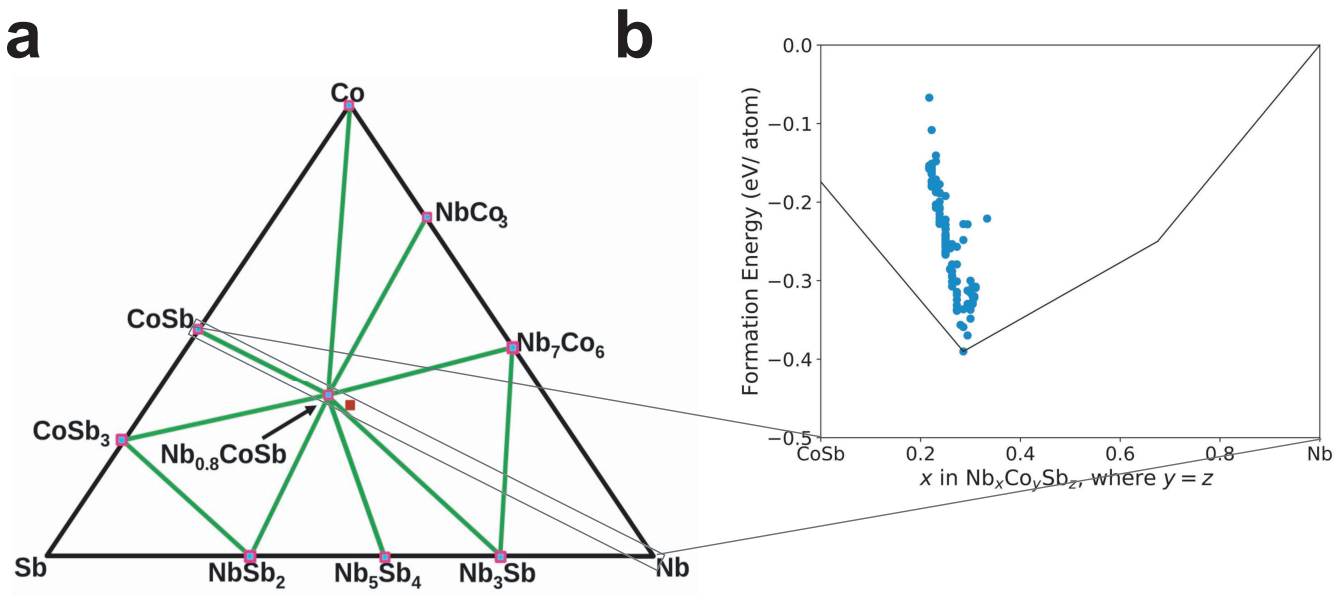

Figure S2: Convex-hull of the Nb-Co-Sb system calculated using[4] DFT along the composition slice CoSb-Nb. The $Nb_{0.8}CoSb$ structure and the defects in it are shown using blue circles.

Numerical proof for defects in ternary compound

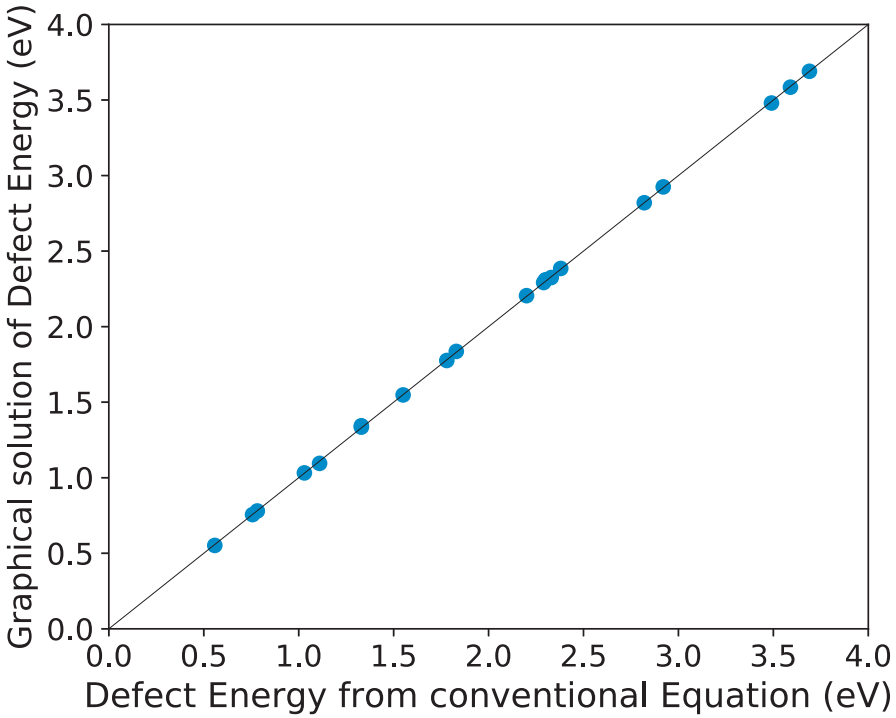

Figure S3: Comparision of defect energies for 20 half-Heusler systems calculated graphically to those determined using conventional defect energy expression

References

(1) Ohno, S.; Imasato, K.; Anand, S.; Tamaki, H.; Kang, S. D.; Gorai, P.; Sato, H. K.; Toberer, E. S.; Kanno, T.; Snyder, G. J. Phase boundary mapping to obtain n-type Mg_3Sb_2-based thermoelectrics. *Joule* **2017**,

(2) Doak, J. W.; Michel, K. J.; Wolverton, C. Determining dilute-limit solvus boundaries in multi-component systems using defect energetics: Na in PbTe and PbS. *Journal of Materials Chemistry C* **2015**, *3*, 10630–10649.

(3) Goyal, A.; Gorai, P.; Peng, H.; Lany, S.; Stevanović, V. A computational framework for

automation of point defect calculations. *Computational Materials Science* **2017**, *130*, 1–9.

(4) Zeier, W. G.; Anand, S.; Huang, L.; He, R.; Zhang, H.; Ren, Z.; Wolverton, C.; Snyder, G. J. Using the 18-Electron Rule To Understand the Nominal 19-Electron Half-Heusler NbCoSb with Nb Vacancies. *Chemistry of Materials* **2017**, *29*, 1210–1217.